Q. J. R. Meteorol. Soc. (1990), **116,** pp. 595–609 551.509.313

A multi-level limited-area slow-equation model: Application to initialization

By PETER LYNCH and A. McDONALD
Meteorological Service, Glasnevin Hill, Dublin 9, Ireland

(Received 14 June 1989; revised 6 October 1989)

SUMMARY

A multi-level limited-area model based on the slow equations is formulated, and applied to the problem of initializing data for a primitive-equation forecast. The slow equations comprise a filtered system whose linear solutions correspond to the low-frequency atmospheric motions. There are no solutions corresponding to the high-frequency gravity-wave solutions of the primitive equations.

The model is used to initialize data for a primitive-equation forecast. It is successful in eliminating high-frequency noise without causing any significant changes in the forecast. The method converges well even when all vertical modes are initialized.

1. INTRODUCTION

In this paper a multi-level limited-area initialization and forecasting model is formulated using the slow equations. These comprise a filtered system of equations in which the high-frequency gravity-wave solutions are absent, and whose low-frequency solutions correspond to the rotational atmospheric motions. The filtering is accomplished by using an approximation similar to that employed in normal-mode initialization: the terms representing the projections of the tendency onto the gravity-wave components are omitted. There results a set of equations in which the rotational components of the flow are determined prognostically whilst appropriate gravity-wave components are determined diagnostically.

The background to the development of the slow system is described in Lynch (1989) and a barotropic version of the equations is derived there. The slow system is closely related to the classical balance system (Charney 1962) but differs at second order in the Rossby number and is free of the spurious solutions of the balance equations. The system models the low-frequency motions which are meteorologically significant, and the evolution of the variables in time is smooth and noise-free.

The model described in this paper has been developed as a component of a system for hourly data assimilation and short-range forecasting. The insertion of observational data which are incompatible with a forecast gives rise to large oscillations in a primitive-equation model. Such data shocks interfere with subsequent data induction cycles. The slow equations may provide a suitable means for the assimilation of observational data during a forecast, as they can absorb inserted data without suffering high-frequency shocks.

As a first step in developing such a system, we derive in section 2 a baroclinic slow-equation model from the primitive equations of a multi-level model. There are two essential approximations involved in the derivation of the slow equations. First, in the divergence equation the term representing the tendency of divergence is set to zero, yielding the balance equation. Second, an equation for the tendency of the deviation from geostrophic balance is derived and the tendency term is then omitted, yielding a diagnostic equation for divergence, which we call the imbalance equation. The system is discretized in such a way that advection is treated in a semi-Lagrangian manner. This has the great advantage of yielding a model with attractive stability characteristics.

In section 3 we apply the slow-equation model to the problem of initializing data for a primitive-equation forecast. The diagnostic components of the slow equations correspond precisely to those used in implicit normal-mode initialization (Bourke and McGregor 1983; Juvanon du Vachat 1986; Temperton 1988). It is shown that the method is successful in eliminating high-frequency noise without causing any significant changes in the forecast. The method converges well, even when all vertical modes are initialized.

Some preliminary forecasts have been made using the slow-equation model. This model is capable of faithfully simulating the evolution of the baroclinic atmospheric flow. Although the quantitative errors are modest, there appear to be some difficulties associated with the boundaries and with the treatment of orography. We hope to report on a more detailed examination of these problems at a future date.

2. Derivation of the baroclinic slow system

(a) *Basic equations and vertical discretization*

The equations of motion for an inviscid dry adiabatic atmosphere may be written as follows (symbols are conventional and are defined in the appendix):

$$\frac{d_{\mathrm{H}}u}{dt} + \frac{1}{a\cos\theta}\frac{\partial G}{\partial \lambda} - \left(f + \frac{u\tan\theta}{a}\right)v = R^u \tag{1}$$

$$\frac{d_{\mathrm{H}}v}{dt} + \frac{1}{a}\frac{\partial G}{\partial \theta} + \left(f + \frac{u\tan\theta}{a}\right)u = R^v \tag{2}$$

$$\frac{d_{\mathrm{H}}T}{dt} - \frac{RT^0}{c_p}\left(\frac{d_{\mathrm{H}}\ln p_{\mathrm{s}}}{dt} + \frac{\dot\sigma}{\sigma}\right) = R^T \tag{3}$$

$$\frac{d_{\mathrm{H}}\ln p_{\mathrm{s}}}{dt} + \delta + \frac{\partial\dot\sigma}{\partial\sigma} = 0 \tag{4}$$

$$\frac{\partial\Phi}{\partial\ln\sigma} = -RT \tag{5}$$

where the horizontal Lagrangian derivative is

$$\frac{d_{\mathrm{H}}}{dt} = \frac{\partial}{\partial t} + \frac{u}{a\cos\theta}\frac{\partial}{\partial\lambda} + \frac{v}{a}\frac{\partial}{\partial\theta}. \tag{6}$$

The temperature T has been separated into a constant part T^0 and a perturbation T' which is small compared to T^0: $T = T^0 + T'$. The modified geopotential G is given by $G = \phi + RT^0\ln p_{\mathrm{s}}$. The nonlinear right-hand terms are given by the following expressions:

$$R^u = \frac{-RT'}{a\cos\theta}\frac{\partial\ln p_{\mathrm{s}}}{\partial\lambda} - \dot\sigma\frac{\partial u}{\partial\sigma}$$

$$R^v = \frac{-RT'}{a}\frac{\partial\ln p_{\mathrm{s}}}{\partial\theta} - \dot\sigma\frac{\partial v}{\partial\sigma}$$

$$R^T = \frac{RT'}{c_p}\left(\frac{\dot\sigma}{\sigma} - \delta - \frac{\partial\dot\sigma}{\partial\sigma}\right) - \dot\sigma\frac{\partial T'}{\partial\sigma}.$$

Vorticity and divergence equations can easily be derived from (1) and (2):

$$Z^{\zeta} \equiv \left(\frac{d_{\mathrm{H}}(\zeta + f)}{dt} + f\delta - R^{\zeta} \right) = 0 \tag{7}$$

$$\frac{\partial \delta}{\partial t} + \nabla^2 G - f\zeta - R^{\delta} = 0 \tag{8}$$

where the vorticity and divergence are given by

$$\zeta = \frac{1}{a \cos\theta} \left(\frac{\partial v}{\partial \lambda} - \frac{\partial u \cos\theta}{\partial \theta} \right)$$

$$\delta = \frac{1}{a \cos\theta} \left(\frac{\partial u}{\partial \lambda} + \frac{\partial v \cos\theta}{\partial \theta} \right)$$

and the nonlinear terms have the following form:

$$R^{\zeta} = \frac{1}{a \cos\theta} \left(\frac{\partial R^{v}}{\partial \lambda} - \frac{\partial R^{u} \cos\theta}{\partial \theta} \right) - \zeta\delta$$

$$R^{\delta} = \frac{1}{a \cos\theta} \left[\frac{\partial}{\partial \lambda} \left\{ -\frac{1}{a \cos\theta} \frac{\partial K}{\partial \lambda} + v\zeta + R^{u} \right\} + \frac{\partial}{\partial \theta} \left\{ \cos\theta \left(-\frac{1}{a} \frac{\partial K}{\partial \theta} - u\zeta + R^{v} \right) \right\} \right]$$

$$- \frac{u}{a} \frac{\partial f}{\partial \theta} + \frac{v}{a \cos\theta} \frac{\partial f}{\partial \lambda}$$

with the kinetic energy density defined by $K = \frac{1}{2}(u^2 + v^2)$. The β-terms in the divergence equation (8) are absorbed into R^{δ} in the same manner as for System D of Temperton (1989).

It is convenient to introduce the vertical discretization at this point. The distribution of variables is shown in Fig. 1. The boundary condition $\dot{\sigma} = 0$ is imposed at the top ($\sigma = \sigma_{\mathrm{T}}$) of the model atmosphere; by definition $\dot{\sigma} = 0$ at the bottom ($\sigma = 1$). After discretization the continuity equation (4) becomes:

$$\left(\frac{d_{\mathrm{H}}}{dt} \right)_l \ln p_{\mathrm{s}} + \delta_l + \frac{\dot{\sigma}_{l+\frac{1}{2}} - \dot{\sigma}_{l-\frac{1}{2}}}{\Delta\sigma_l} = 0. \tag{9}$$

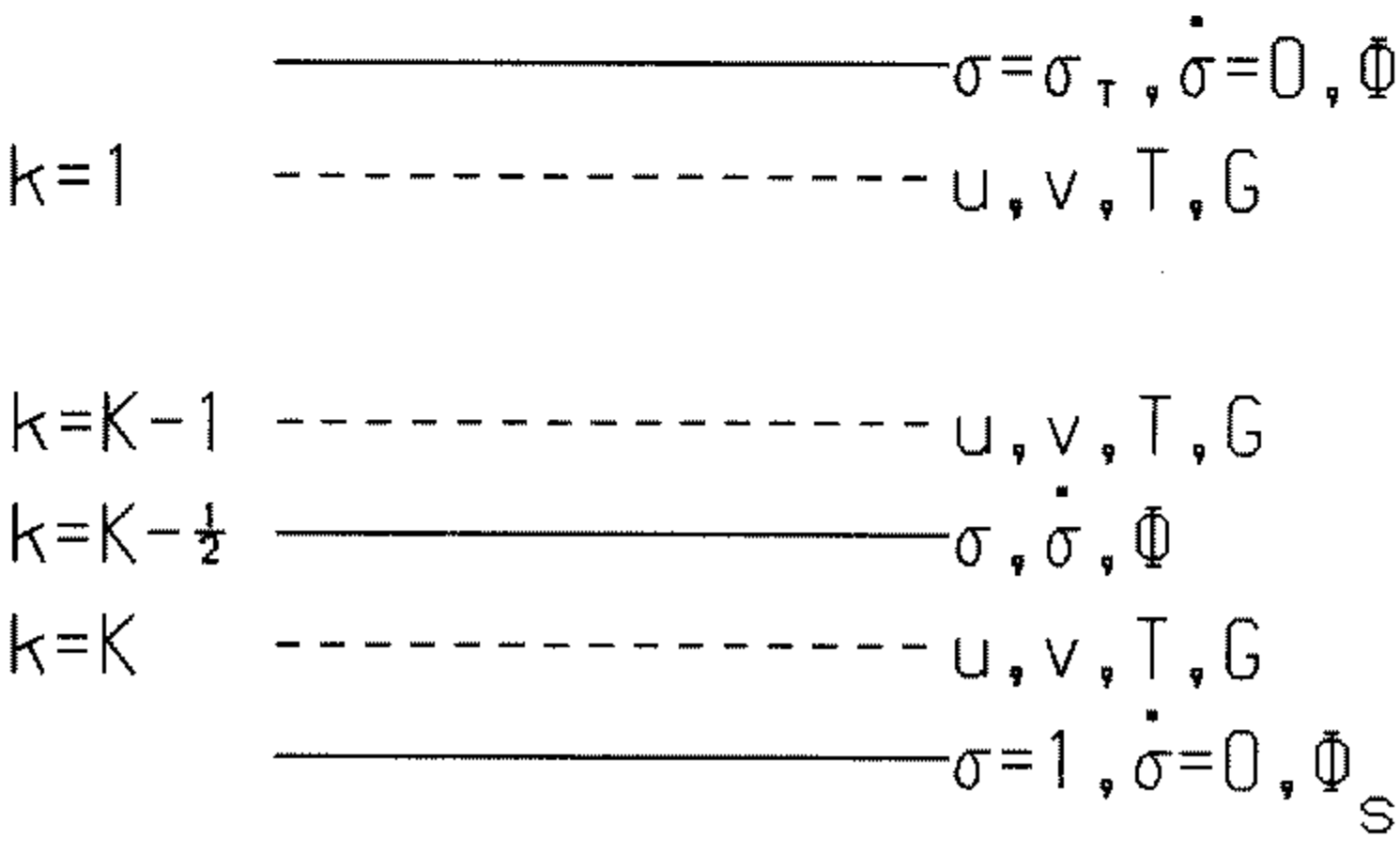

Figure 1. Distribution of the variables in the vertical direction.

Total and partial vertical summations of (9), using the boundary conditions, yield

$$\sum_{l=1}^{K} \Delta\sigma_l \left\{ \left(\frac{d_{\mathrm{H}}}{dt} \right)_l \ln p_{\mathrm{s}} + \delta_l \right\} = 0 \tag{10}$$

and

$$\bar{\dot{\sigma}}_k = \sum_{l=1}^{K} \Delta\sigma_l \left\{ \left(\frac{d_{\mathrm{H}}}{dt} \right)_l \ln p_{\mathrm{s}} + \delta_l \right\} J_{kl} \tag{11}$$

where, for any variable Ψ, a vertical average is defined by $\bar{\Psi}_k = \frac{1}{2}(\Psi_{k-\frac{1}{2}} + \Psi_{k+\frac{1}{2}})$ and the matrix **J** is upper triangular, with elements defined as follows:

$$J_{kl} = 1 \qquad k < l$$

$$J_{kl} = \tfrac{1}{2} \qquad k = l$$

$$J_{kl} = 0 \qquad k > l.$$

Summing the hydrostatic equation (5) in the vertical and using $G_k = \bar{\Phi}_k + RT^0 \ln p_{\mathrm{s}}$ yields

$$G_k = \Phi_{\mathrm{s}} + RT^0 \ln p_{\mathrm{s}} + \sum_{l=k}^{K}{}' RT_l \ \Delta \ln \sigma_l \tag{12}$$

where Φ_{s} is the surface geopotential and the primed summation notation is defined by

$$\sum_{l=k}^{K}{}' \Psi_l = \tfrac{1}{2}\Psi_k + \sum_{l=k+1}^{K} \Psi_l.$$

In order to proceed with the derivation, which hinges on using the variable G rather than T, the thermodynamic equation (3) is partially summed in the vertical:

$$Z^G \equiv \sum_{l=k}^{K}{}' R\Delta \ln \sigma_l \ \left\{ \left(\frac{d_{\mathrm{H}}}{dt} \right)_l \left[T_l - \frac{RT^0}{c_p} \ln p_{\mathrm{s}} \right] - R_l^T \right\} + \sum_{l=1}^{K} M_{kl} \left\{ \left(\frac{d_{\mathrm{H}}}{dt} \right)_l \ln p_{\mathrm{s}} + \delta_l \right\} = 0. \tag{13}$$

In arriving at this result, (11) has been substituted in the discrete form of (3) and the integrated mass equation (10) has been used. The vertical coupling matrix **M** is defined by

$$M_{kl} = \left[\left(\frac{RT^0}{1-\sigma_{\mathrm{T}}} \right) + \frac{R^2 T^0}{c_p} \sum_{m=k}^{K}{}' \left(\frac{\Delta \ln \sigma_m}{\bar{\sigma}_m} \right) \left\{ \frac{1}{1-\sigma_{\mathrm{T}}} - J_{ml} \right\} \right] \Delta\sigma_l. \tag{14}$$

It is straightforward to show that **M** has the following property:

$$\sum_{l=1}^{K} M_{kl} = RT^0 \left[1 + \frac{R}{c_p} \sum_{l=k}^{K}{}' \Delta \ln \sigma_l \right]. \tag{15}$$

(*b*) *Derivation of the slow equations*

The scene is now set for deriving a slow system of equations. Firstly, setting $\partial\delta/\partial t = 0$ in the divergence equation (8) yields a diagnostic equation involving G and ζ, the so-called balance equation

$$\nabla^2 G_k - f\zeta_k = R_k^{\delta} \tag{16}$$

which is the multi-level analogue of Lynch's (1989) Eq. (17).

Secondly, the multi-level analogue of Lynch's (1989) Eq. (18), the so-named imbalance equation, can be obtained by deriving an equation for the tendency of geostrophic imbalance, $\varepsilon \equiv (\nabla^2 G_k - f\zeta_k)$, and then omitting the tendency term. To accomplish this, we combine (7) and (13) as follows: $\nabla^2 Z_k^G - f Z_k^\zeta = 0$. Using (6) and (12) and property (15) of the matrix **M** gives

$$\frac{\partial}{\partial t}(\nabla^2 G_k - f\zeta_k) + \nabla^2 \sum_{l=1}^{K} M_{kl}\delta_l - f^2\delta_k = A_k^{\mathrm{I}} \tag{17}$$

where $A_k^{\mathrm{I}} = \nabla^2 A_k^G - f A_k^\zeta$ with

$$A_k^G = \sum_{l=k}^{K}{}' R\Delta \ln \sigma_l \left\{ -\mathbf{v}_l \cdot \boldsymbol{\nabla}\left(T_l - \frac{RT^0}{c_p}\ln p_s\right) + R_l^T \right\} - \sum_{l=1}^{K} M_{kl}\mathbf{v}_l \cdot \boldsymbol{\nabla} \ln p_s$$

and $A_k^\zeta = R_k^\zeta - \mathbf{v}_k \cdot \boldsymbol{\nabla}(\zeta_k + f)$. If the tendency term is omitted, (17) becomes a diagnostic equation for the divergence.

The vertical levels are coupled through the matrix **M**. To separate them, let **E** be the matrix whose columns are the eigenvectors of **M**, and **Λ** the diagonal eigenvalue matrix, so that

$$\mathbf{E}^{-1}\mathbf{M}\mathbf{E} = \boldsymbol{\Lambda}. \tag{18}$$

We denote the vertical transform of a variable Ψ by a tilde:

$$\tilde{\Psi} = \sum_{l=1}^{K} (E^{-1})_{kl}\Psi_l.$$

Now, pre-multiplying (17) by $\mathbf{E}^{-1}$ and omitting the tendency term, we obtain a diagnostic equation for δ:

$$(\Lambda_k \nabla^2 - f^2)\tilde{\delta}_k = \tilde{A}_k^{\mathrm{I}} \tag{19}$$

where Λ_k is the kth eigenvalue of **M**. We call (19) the imbalance equation. It is the multi-level analogue of Eq. (18) in Lynch (1989).

Next, a prognostic equation involving ζ and G is obtained by eliminating δ between the vorticity equation (7) and the (summed) thermodynamic equation (13), which yields

$$f\left[\sum_{l=k}^{K}{}' R\Delta \ln \sigma_l \left\{\left(\frac{d_{\mathrm{H}}}{dt}\right)_l \left(T_l - \frac{RT^0}{c_p}\ln p_s\right) - R_l^T\right\} + \sum_{l=1}^{K} M_{kl}\left(\frac{d_{\mathrm{H}}}{dt}\right)_l \ln p_s\right]$$

$$- \sum_{l=1}^{K} M_{kl}\left[\frac{d_{\mathrm{H}}(\zeta + f)}{dt} - R^\zeta\right]_l = 0. \tag{20}$$

In order to maximize the allowable time-step, the time discretization is performed in a semi-Lagrangian fashion. For any variable $\Psi(\lambda, \theta, t)$, we denote by an asterisk the value of the variable at a departure point at time $n\Delta t$:

$$\Psi_*^n = \Psi(\lambda - \hat{u}\Delta t/a\cos\theta, \theta - \hat{v}\Delta t/a, n\Delta t) \tag{21}$$

corresponding to the parcel arriving at point (λ, θ) at time $(n+1)\Delta t$. Here $(\hat{u}, \hat{v})$ is the centred in space and time velocity (McDonald and Bates 1987). Using property (15) of the matrix **M**, (20) can then be written

$$fG_k^{n+1} - \sum_{l=1}^{K} M_{kl}\,\zeta_l^{n+1} = C_k^V \tag{22}$$

where

$$C_k^V = f\left[\Phi_s + \sum_{l=k}^{K}{}' R\Delta \ln \sigma_l \, (C^T)^n_{*,l} + \sum_{l=1}^{K} M_{kl}(\ln p_s)^n_{*,l}\right] - \sum_{l=1}^{K} M_{kl}[(C^\zeta)^n_{*,l} - f]$$

with

$$C_l^T = T_l - \frac{RT^0}{c_p}\ln p_s + \Delta t \cdot R_l^T$$

and

$$C_l^\zeta = \zeta_l + f + \Delta t \cdot R_l^\zeta.$$

If (22) is pre-multiplied by $\mathbf{E}^{-1}$ and use made of (18) we obtain

$$f\tilde{G}_k^{n+1} - \Lambda_k \xi_k^{n+1} = C_k^V. \tag{23}$$

This constitutes the first prognostic equation and relates G and ζ at time $(n+1)\Delta t$. Equation (23) is a form of the potential vorticity equation.

It remains to derive a prognostic equation relating $\ln p_s$ and ζ. This can be done by eliminating δ between the continuity equation (10) and the vorticity equation (7):

$$\sum_{l=1}^{K} \Delta\sigma_l \left\{\frac{d_H(\zeta + f)}{dt} - R^\zeta - f\left(\frac{d_H \ln p_s}{dt}\right)\right\}_l = 0. \tag{24}$$

Again, discretizing in time in a semi-Lagrangian fashion yields

$$\sum_{l=1}^{K} \Delta\sigma_l\{\xi_l^{n+1} + f - f\ln p_s^{n+1} - (C^\zeta)^n_{*,l} + f(\ln p_s)^n_{*,l}\} = 0$$

or

$$f(1-\sigma_T)\ln p_s^{n+1} = \sum_{l=1}^{K} \Delta\sigma_l\{\xi_l^{n+1} + f - (C^\zeta)^n_{*,l} + f(\ln p_s)^n_{*,l}\}. \tag{25}$$

This concludes the derivation of the slow system of equations. The system comprises the two prognostic equations (23) and (25) and the diagnostic balance and imbalance equations (16) and (19). To complete the system we use the continuity equation (9) diagnostically for the vertical velocity, that is

$$\dot{\sigma}^{n+1}_{k-\frac{1}{2}} = \sum_{l=k}^{K} \Delta\sigma_l \left\{\left(\frac{\partial}{\partial t}\right)\ln p_s + \mathbf{v}_l \cdot \boldsymbol{\nabla} \ln p_s + \delta_l\right\}^{n+1} \tag{26}$$

where

$$\left\{\left(\frac{\partial}{\partial t}\right)\ln p_s\right\}^{n+1} = -\frac{1}{1-\sigma_T}\sum_{l=1}^{K} \Delta\sigma_l\{\mathbf{v}_l \cdot \boldsymbol{\nabla}\ln p_s + \delta_l\}^{n+1}.$$

(c) *Numerical solution of the slow system*

The method of solution will now be described. The slow system comprises prognostic and diagnostic elements. In the context of forecasting, the prognostic components are

used to advance the variables from time-level $n\Delta t$ to $(n+1)\Delta t$. In this paper we restrict attention to the application of the slow system to initialization. In that case, the first step below, the semi-Lagrangian step, is omitted, the time-step Δt is taken as zero and the index n may be interpreted as an iteration count.

The first step of the integration (omitted for initialization) is the semi-Lagrangian step. This is performed by estimating the departure-point values of the terms $\ln p_s$, C^T and C^ζ by means of a bi-cubic interpolation using the surrounding gridpoint values. Having completed this, the values of $(\ln p_s)^n_*$, $(C^T)^n_*$ and $(C^\zeta)^n_*$ associated with the G-type arrival points interior to the solid line in Fig. 2 are known.

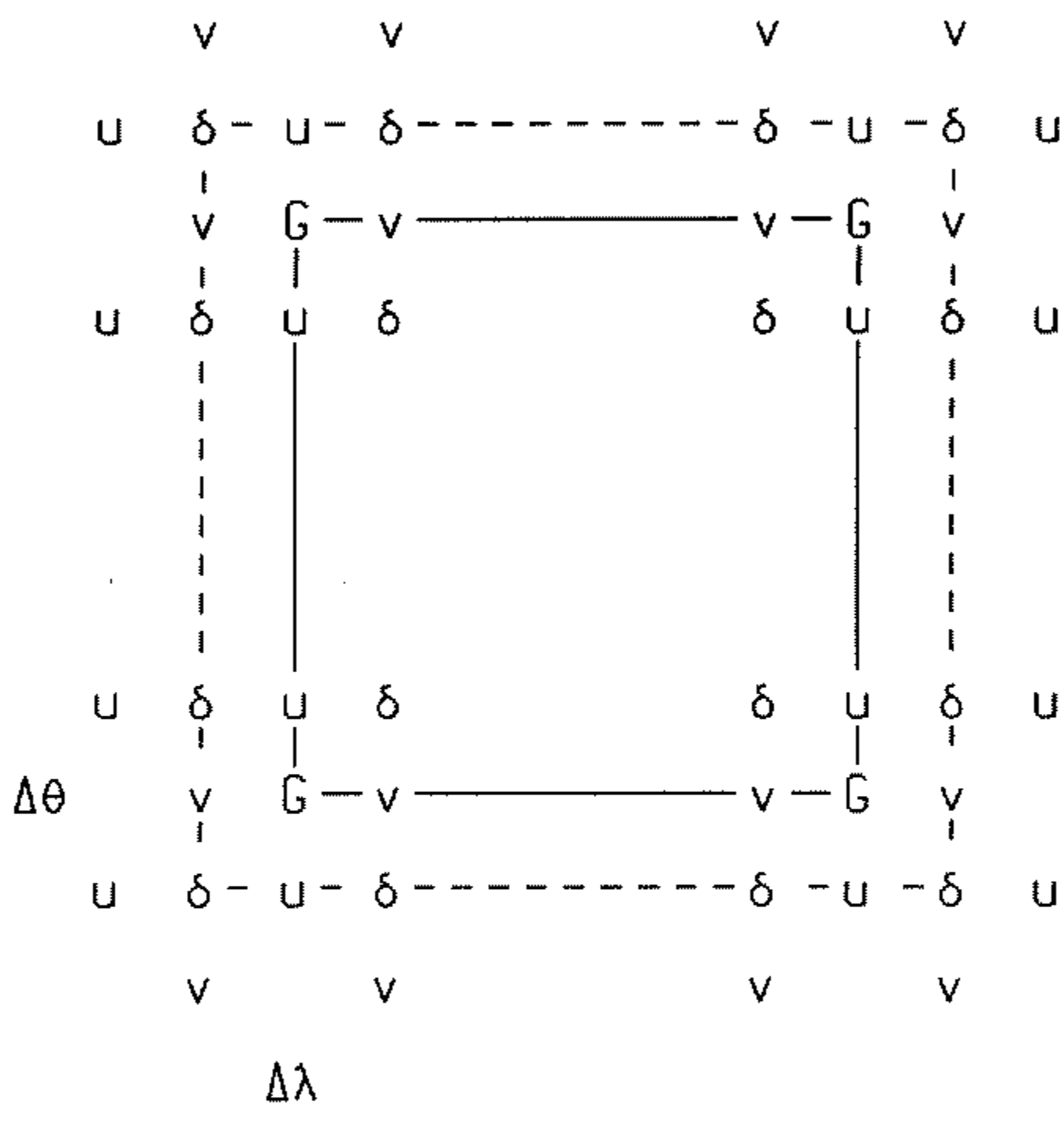

Figure 2. Distribution of the variables on the horizontal D-grid. The solid line is the boundary for geopotential and normal wind.

In the second step of the integration $\tilde{G}^{n+1}$ is calculated. This can be accomplished by eliminating ζ^{n+1} from (16) and (23) to yield a Helmholtz equation for $\tilde{G}$:

$$(\nabla^2 - f^2/\Lambda_k)\tilde{G}^{n+1}_k = \tilde{R}^\delta_k - f\tilde{C}^V_k/\Lambda_k. \tag{27}$$

As a result of step 1, $\tilde{C}^V_k$ can be computed. In addition it is necessary, in principle, to know $\tilde{R}^\delta_k$ at time-level $n+1$ in order to solve (27). In practice, it must be approximated by its value at time $n\,\Delta t$. Since it consists of nonlinear terms, the resulting error should be small. Dirichlet boundary conditions are used in solving (27), with the values of $\tilde{G}$ specified at the points along the solid line in Fig. 2.

Once $\tilde{G}^{n+1}$ is known, $\tilde{\zeta}^{n+1}$ follows from (23), and this in turn yields $\ln p_s^{n+1}$ from (25) and then T^{n+1} from (12). We now know the mass field at time-level $(n+1)\Delta t$, or iteration number $(n+1)$ in the case of initialization.

In the third step of the integration the imbalance equation (19) is solved for $\tilde{\delta}^{n+1}$. Again it is necessary in principle to know A^I_k at time $(n+1)$. In practice, because $\mathbf{V}^{n+1}$ is not yet known, this is not possible. However, if a term in A^I_k is known at the new time-

level, it is used. In solving (19) the homogeneous Dirichlet condition $\tilde{\delta} = 0$ is applied on the dashed line in Fig. 2.

In the second and third steps a Helmholtz equation of the form

$$[\nabla^2 - A(\lambda, \theta)]\Psi(\lambda, \theta) = B(\lambda, \theta) \tag{28}$$

with A positive, must be solved. The method used is analogous to that of Concus and Golub (1973) in that, instead of (28), the following iterative equation is solved:

$$[\nabla^2 - \overline{A}]\Psi^{k+1} = B(\lambda, \theta) - [\overline{A} - A(\lambda, \theta)]\Psi^k \tag{29}$$

where $\overline{A}$ is the areal average of $A(\lambda, \theta)$. Four iterations of a fast solver (Sweet 1977) were found to give satisfactory convergence.

In the fourth step of the integration u^{n+1} and v^{n+1} are recovered from ζ^{n+1} and δ^{n+1}. This requires that a component of the wind on the boundary be specified. The method used is that of Sangster (1960), discussed in detail in Lynch (1988). We introduce a streamfunction ψ and velocity potential χ:

$$u = \frac{1}{a\cos\theta}\frac{\partial\chi}{\partial\lambda} - \frac{1}{a}\frac{\partial\psi}{\partial\theta} \tag{30}$$

$$v = \frac{1}{a\cos\theta}\frac{\partial\psi}{\partial\lambda} + \frac{1}{a}\frac{\partial\chi}{\partial\theta} \tag{31}$$

which, when differentiated, give

$$\nabla^2\chi = \delta \tag{32}$$

$$\nabla^2\psi = \zeta. \tag{33}$$

These Poisson equations are solved using the fast method of Sweet (1977) to yield χ^{n+1} and ψ^{n+1}. Subsequently, u^{n+1} and v^{n+1} are recovered by means of (30) and (31). In solving the Poisson equation for χ the boundary condition $\chi = 0$ is applied on the dashed line in Fig. 2. A boundary condition for ψ is derived using the normal component of the wind on the boundary: the equation

$$V_n = -\frac{\partial\psi}{\partial s} + \frac{\partial\chi}{\partial n} \tag{34}$$

is integrated along the solid line in Fig. 2 using the known normal gradient of χ on this line to yield the streamfunction as a function of boundary position. In order that this process should yield a single-valued streamfunction, it is necessary that the input data satisfy the following integral constraint:

$$\iint_{\Omega} \delta \; da = \oint_{\partial\Omega} V_n \, ds. \tag{35}$$

To ensure this, the normal boundary wind is adjusted by the addition of a (normally small) constant.

The fifth and final step of the integration is the calculation of the vertical velocity $\dot{\sigma}^{n+1}$ by means of (26).

A multi-level model, LASER, has been coded to solve the equations developed in this section. It is run on a limited area using a transformed latitude/longitude grid, with pole at the geographic position 30°N 150°E, and resolution $\Delta\lambda = \Delta\theta = 2°$. There are 40×26 points covering the area shown in Fig. 3. There are five vertical levels, with an upper boundary at $\sigma = 0{\cdot}2$. In order that G and ζ points coincide, a D-grid is used, with u and v specified half a grid-step north and east respectively of G (see Fig. 2).

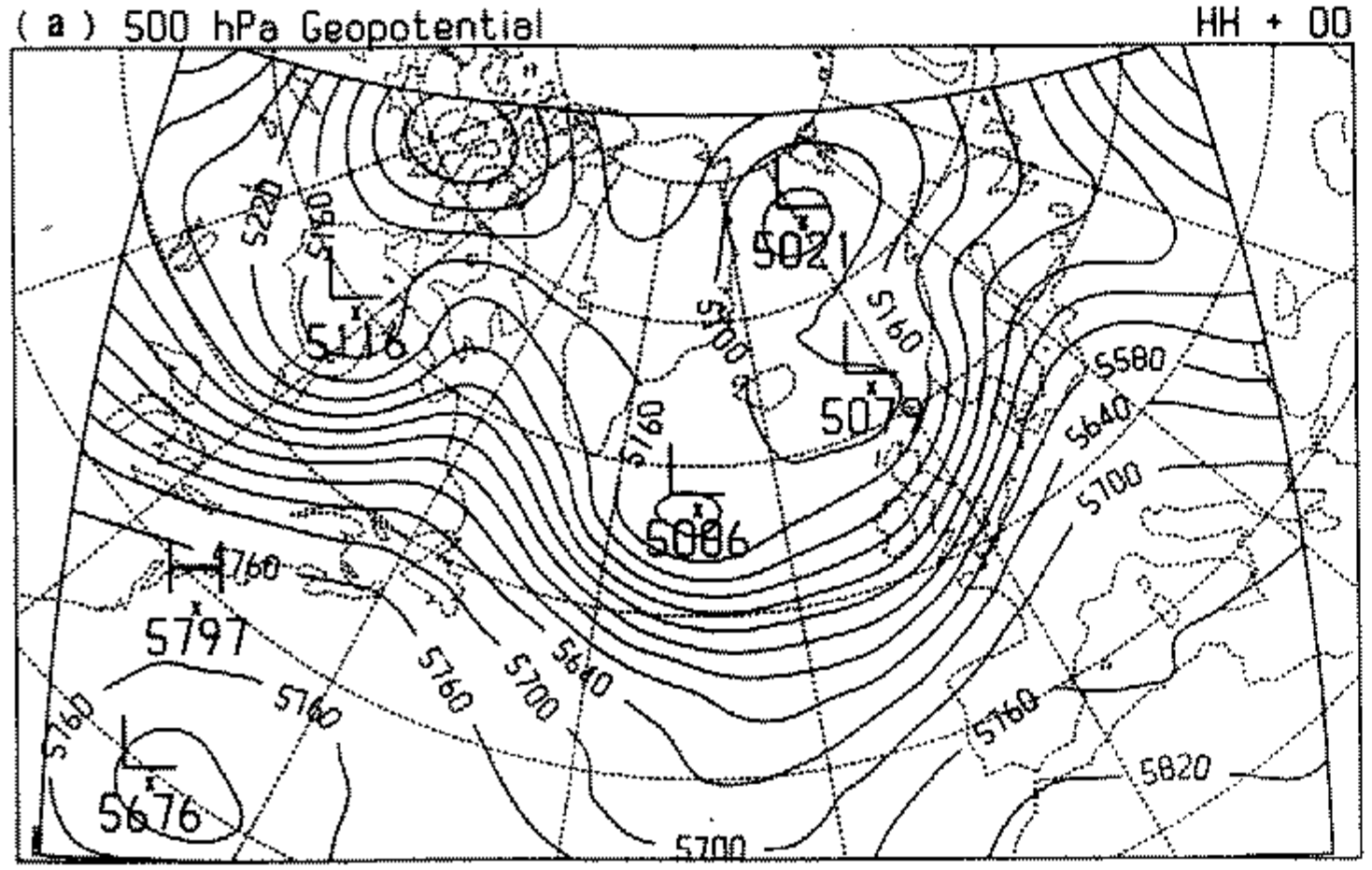

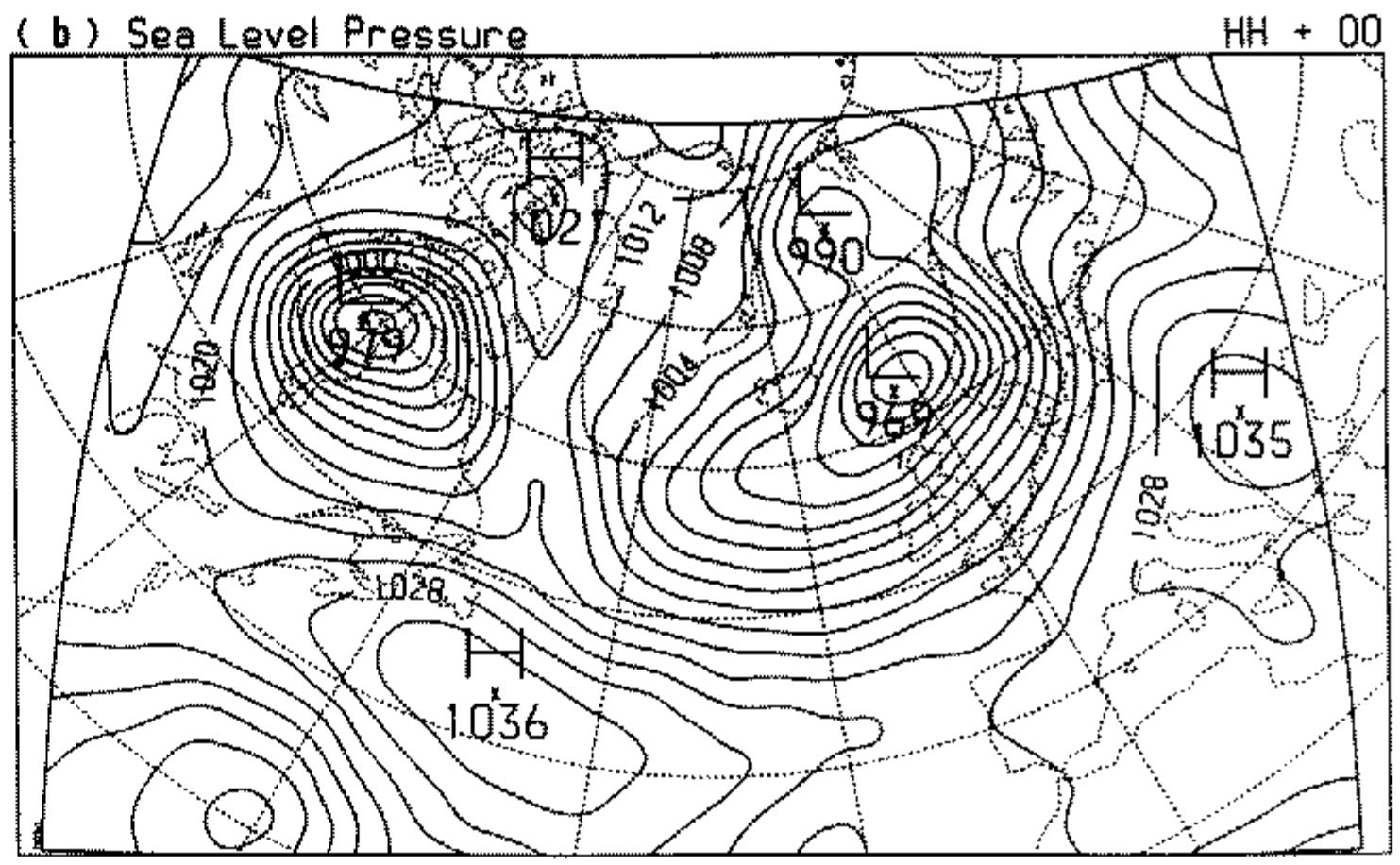

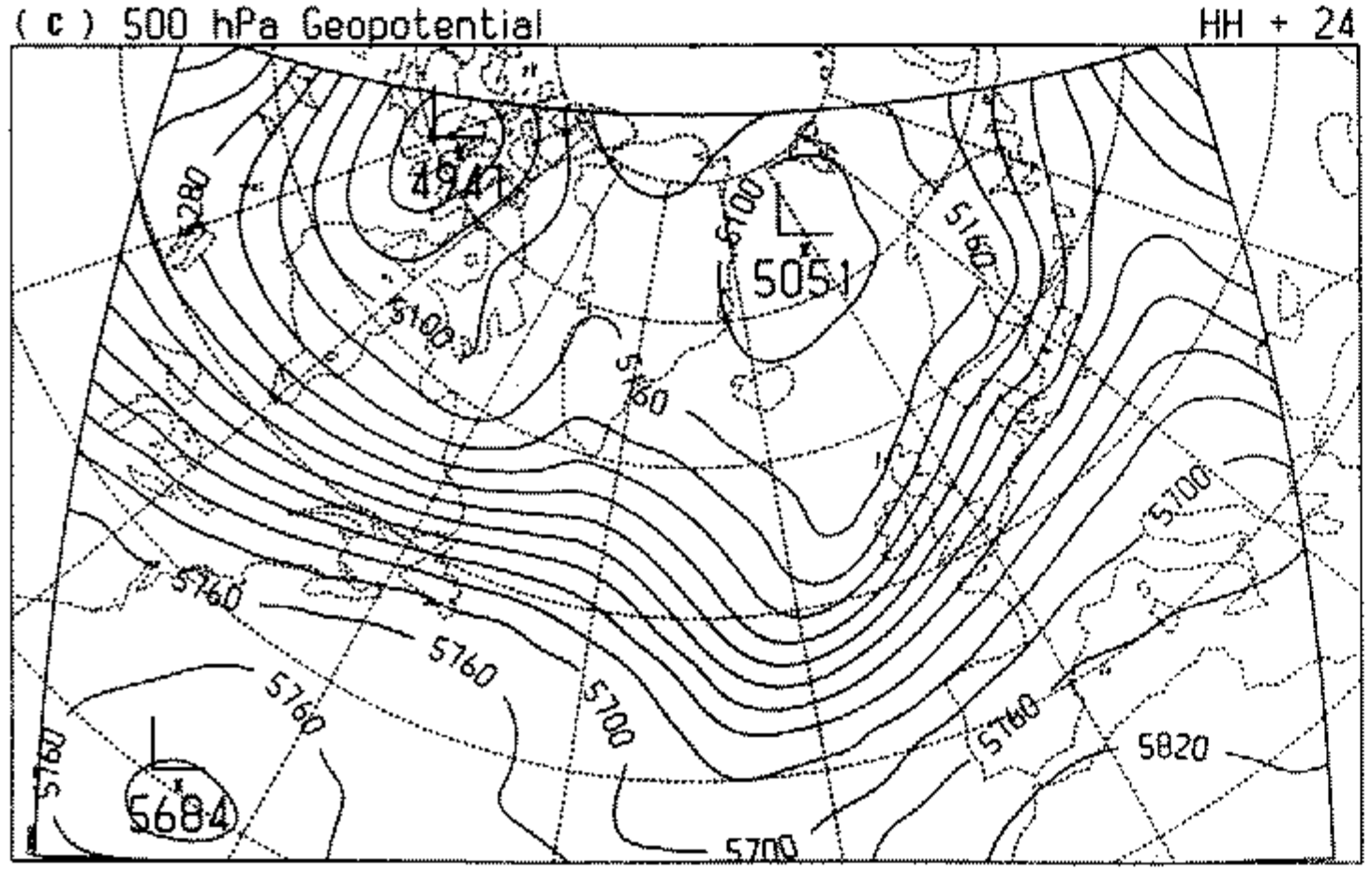

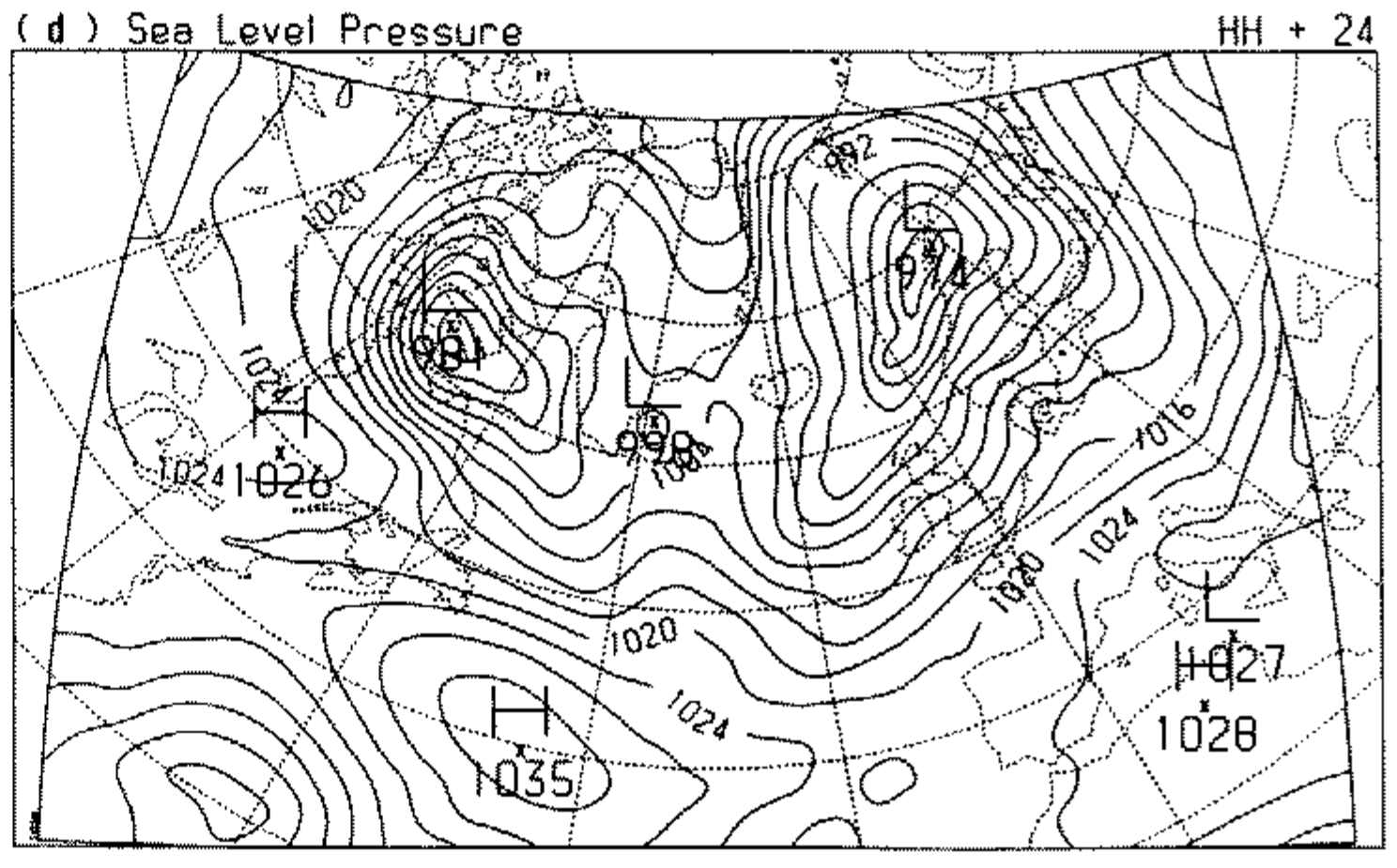

Figure 3. Initial data valid at 0000 UTC 22 November 1982 and 24-hour forecasts from these data. (a), (b) Initial 500 hPa geopotential and sea-level pressure. (c), (d) Corresponding 24-hour forecast fields.

3. Initialization

Nonlinear normal-mode initialization is an effective way to define balanced initial fields (Machenhauer 1977). An implicit formulation of normal-mode initialization (we denote it INMI) has been developed (Bourke and McGregor 1983; Juvanon du Vachat 1986; Temperton 1988). The essence of INMI is to reformulate the primitive equations in such a way that the tendencies of gravity-wave components occur as explicit terms, and to derive diagnostic relationships by omitting these terms. The diagnostic equations derived in section 2 above are analogous to those of scheme B of Bourke and McGregor (1983) and system D of Temperton (1989).

Temperton (1988) used INMI with a barotropic regional model, and showed that it eliminates the high-frequency oscillations. We have extended this method to the baroclinic case using the slow-equation model LASER. In this section we describe initialization experiments using LASER, corresponding to a multi-level formulation of INMI. The assumptions made in deriving the slow equations are the same as for INMI, and the resulting diagnostic relationships are similar. Each time-step of LASER involves a semi-Lagrangian advection and an adjustment component. If the time interval is set to zero each time-step corresponds exactly to a single iteration of an INMI scheme. In (23) and (25) the departure point quantities are evaluated at the arrival points. In (16), (19) and (26) the advection terms are explicitly included. The initialization is performed by running LASER for two time-steps with $\Delta t = 0$, corresponding to two iterations of nonlinear normal-mode initialization of all vertical modes.

The forecast model used for the initialization experiments is described in McDonald (1986). It uses a semi-Lagrangian advection step and a semi-implicit adjustment step. A C-grid is used, with u and v specified a half grid-step east and north respectively of Φ. Since LASER uses a D-grid, with the positions of u and v interchanged, the initialized winds must be interpolated to the C-grid before the forecast can be made. The vertical levels of the forecast model are the same as those of the initialization scheme (see Fig. 1), and the two models have the same equivalent depths and vertical normal modes. For the forecast experiments described here, the geopotential was held constant on the boundary. All wind and mass values interior to this boundary were updated during the forecast.

The initial data are the analyses of mass and wind valid at 0000 UTC, 22 November 1982. The 500 hPa geopotential and sea-level pressure are seen in Figs. 3(a) and 3(b). The 24-hour forecasts from these fields are shown in Figs. 3(c) and 3(d). The initialized fields and the forecasts resulting from them look similar to those in Fig. 3 and it is more useful to plot the difference fields. In Figs. 4(a) and 4(b) the changes in 500 hPa height and sea-level pressure are plotted. The differences in these fields at 24 hours between the initialized and uninitialized runs are seen in Figs. 4(c) and 4(d). The maximum change in 500 hPa height is 22 m (the contour interval in Figs. 4(a) and 4(c) is 10 m). The largest change in surface pressure is 2·6 hPa (the contour interval in Figs. 4(b) and 4(d) is 1 hPa). The differences between the 24-hour forecasts, shown in Figs. 4(c) and 4(d), are slightly smaller than those of the initial fields, with maximum differences in 500 hPa height and surface pressure of 19 m and 1·8 hPa respectively. There is some evidence of a large-scale pattern of error in Fig. 4(c). This may be due to the treatment of the β-terms, as discussed in Temperton (1989).

The r.m.s. changes in surface pressure and 500 hPa height due to initialization are 0·58 hPa and 6·2 m. The corresponding differences between the two forecasts are 0·53 hPa and 5·0 m. The r.m.s. change in the wind field, averaged in the vertical, is $3{\cdot}3\,\mathrm{m\,s^{-1}}$. The corresponding r.m.s. difference between the forecasts is $1{\cdot}9\,\mathrm{m\,s^{-1}}$. It is

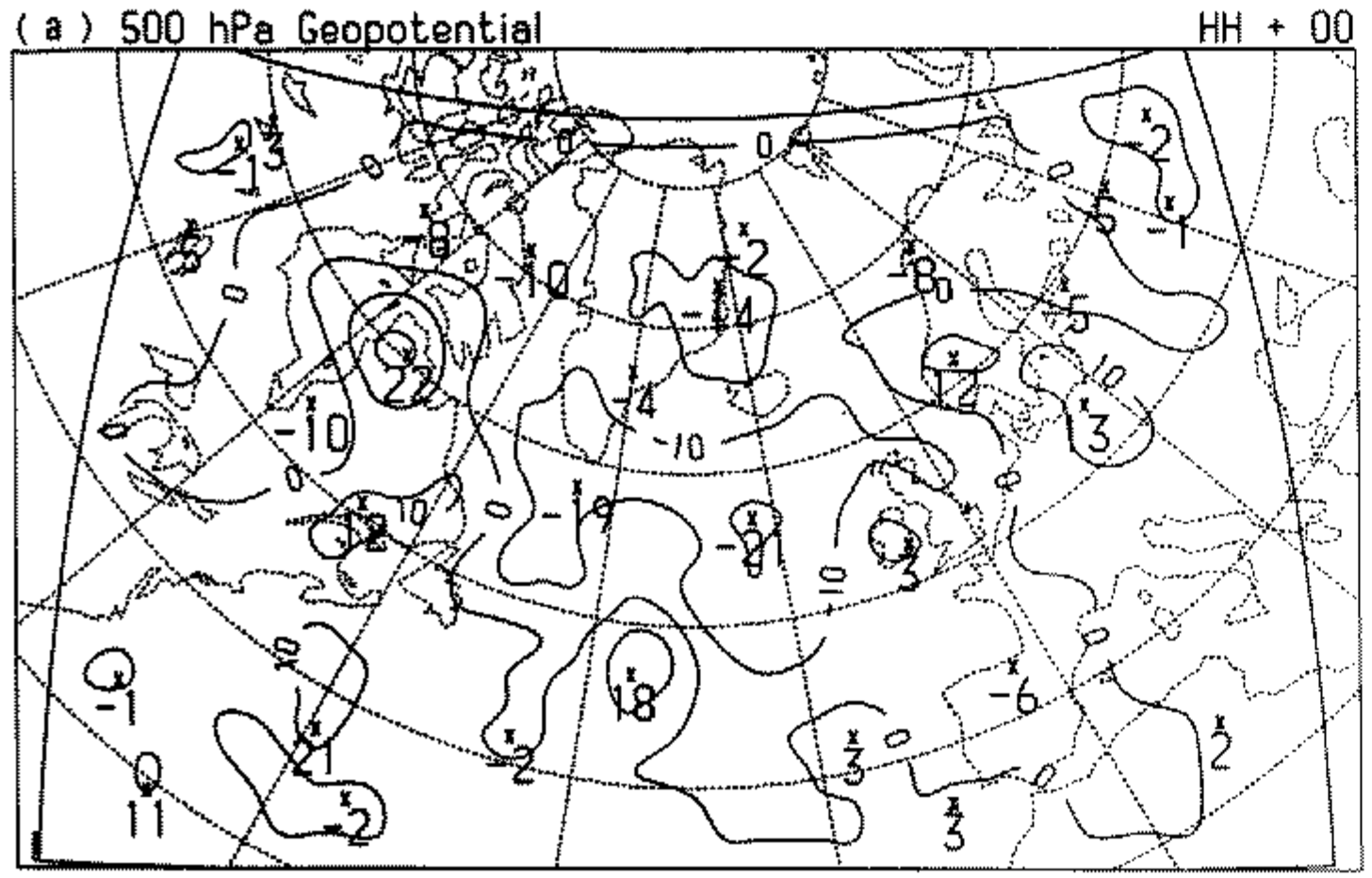

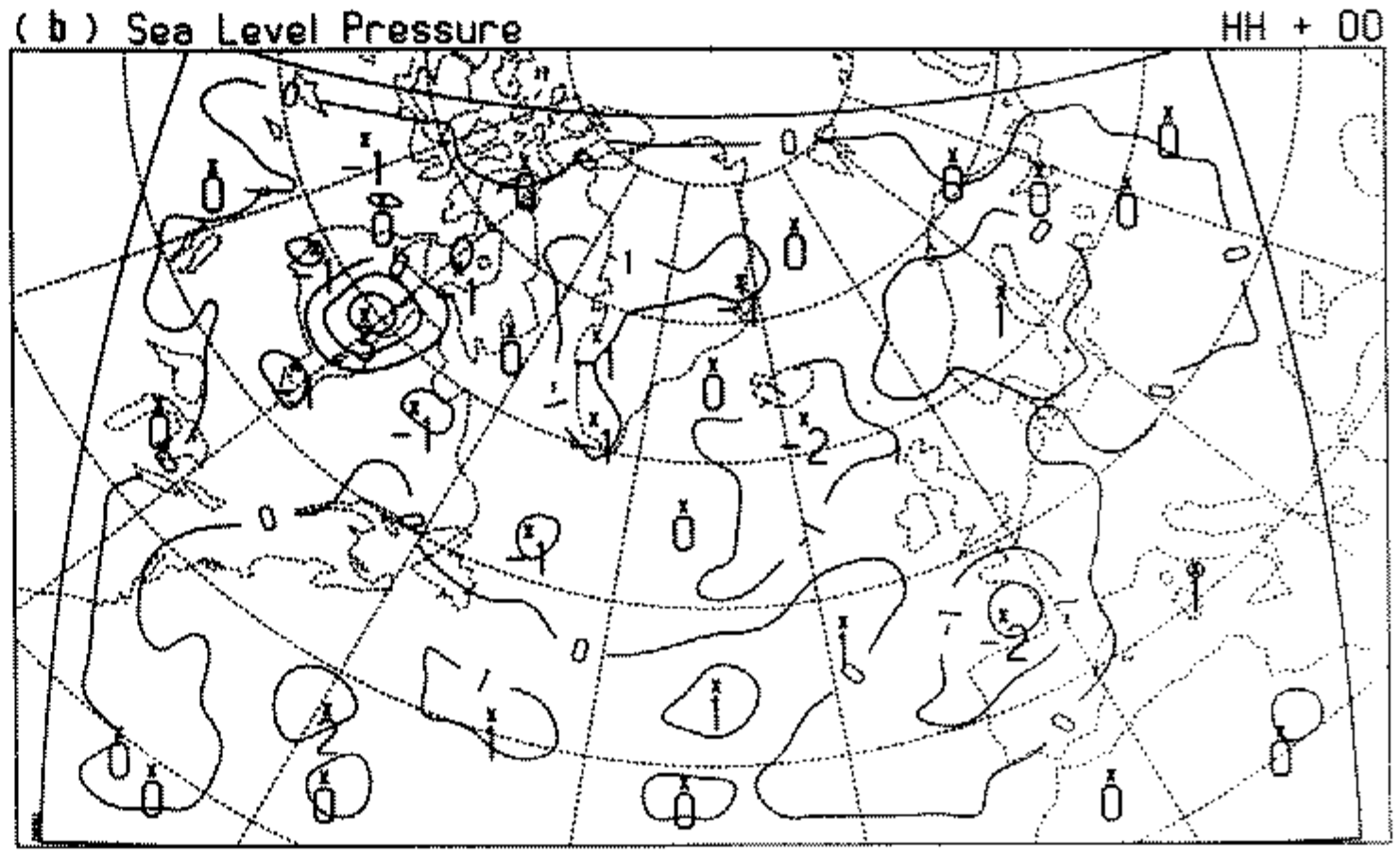

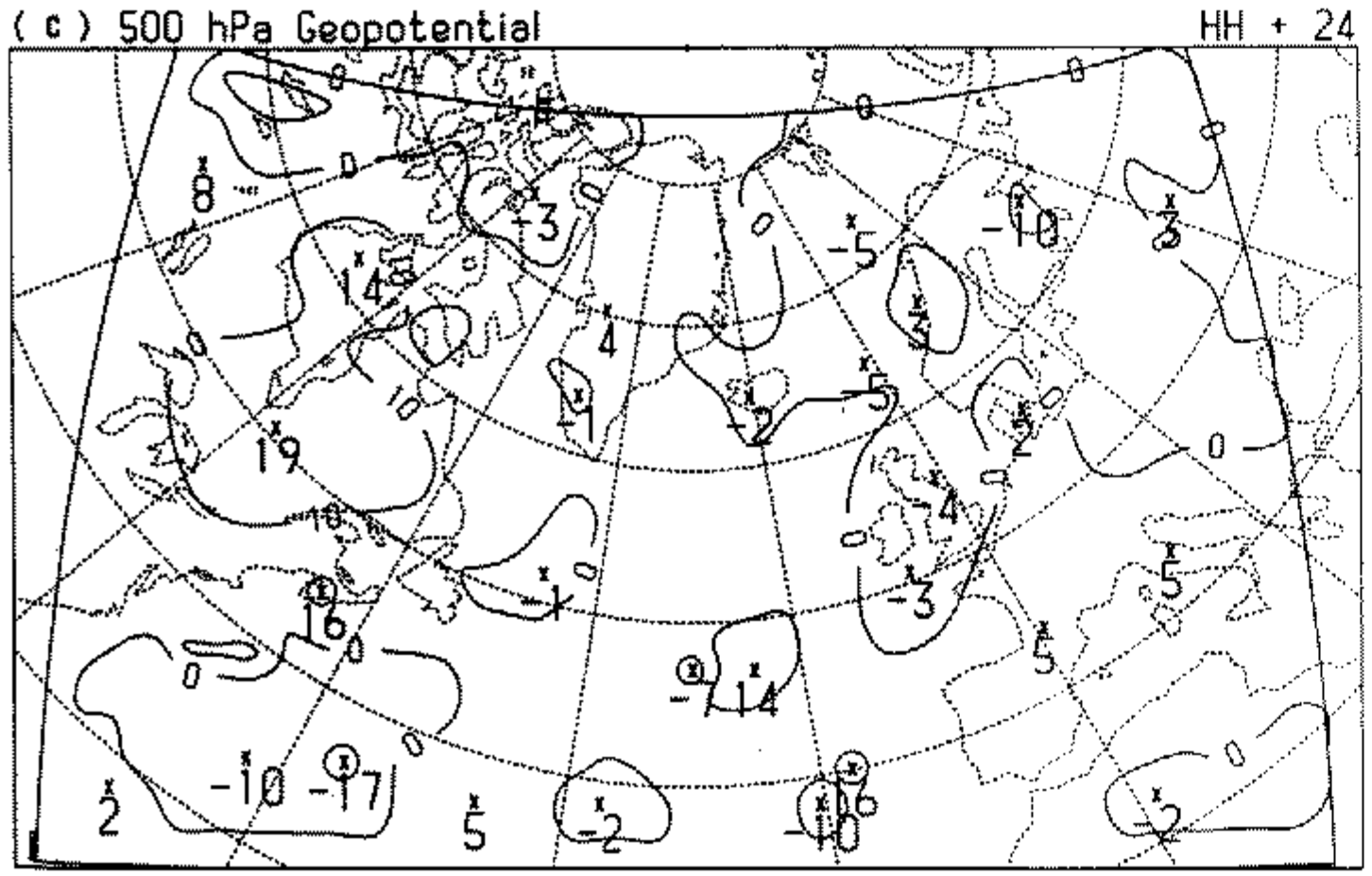

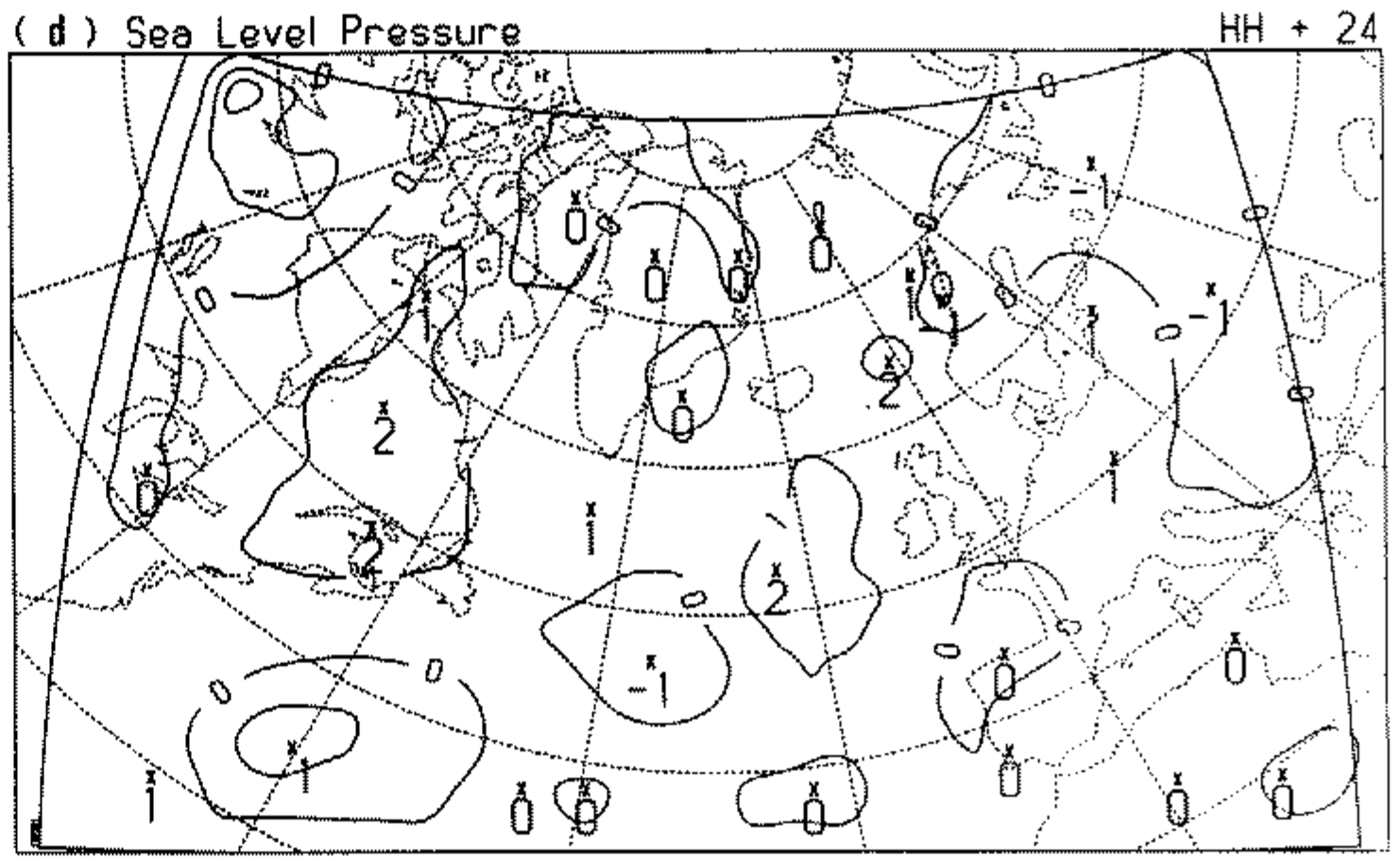

Figure 4. (a), (b) Differences between the initialized and uninitialized analyses of 500 hPa geopotential and sea-level pressure. (c), (d) Differences in the 500 hPa geopotential and sea-level pressure, between forecasts starting from initialized and uninitialized analyses.

clear that the changes induced in the analysed fields by the initialization result in acceptably small changes in the forecast.

The effect of initialization on the evolution of the forecasts can be seen by plotting the surface pressure at a single point. The solid line in Fig. 5(a) shows the pressure for the uninitialized run. The dashed line, for the initialized run, is very much smoother and the initial shock is absent. The mean absolute divergence provides a global indicator of gravity-wave noise. The evolution of this quantity before and after initialization, shown in Fig. 5(b), confirms the effectiveness of the initialization procedure in removing high-frequency noise.

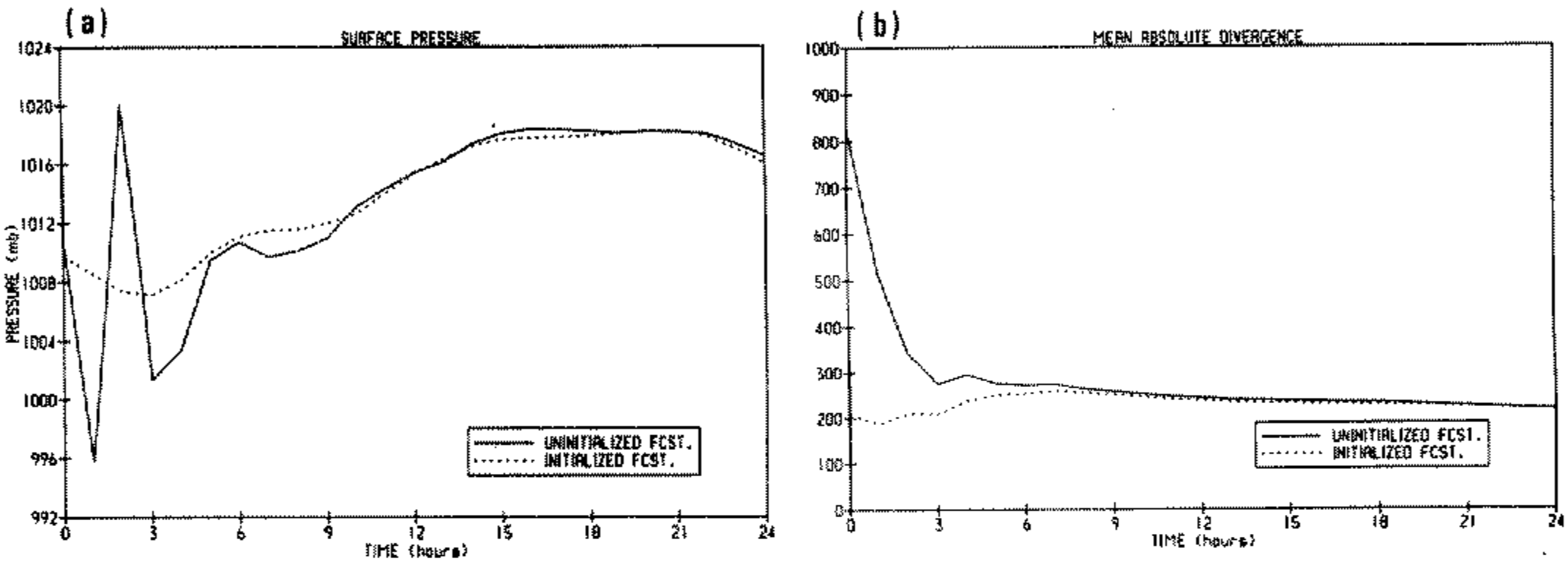

Figure 5. (a) Evolution of the surface pressure at a central point (19, 9) starting from uninitialized data (solid) and initialized data (dotted). (b) Corresponding curves for the absolute divergence averaged over the forecast area (units $10^{-8}s^{-1}$).

The mean absolute divergence before initialization was 833 (in units of $10^{-8}s^{-1}$). After initialization this was reduced to 200. Since LASER uses a D-grid, interpolation back to the forecast model C-grid was necessary and this increased the mean absolute divergence to 208. The value at the end of the 24-hour forecast was 218. Divergence damping (with a coefficient $C_\delta = 3{\cdot}4\times10^7 m^2 s^{-1}$) was applied in both the uninitialized and initialized forecasts. It was not necessary in the initialized run, but was included to make the correspondence between the runs as close as possible.

Most initialization procedures are applied only to the vertical modes of largest scales and higher internal modes are left unaltered. Non-convergence of the iterative process for the higher modes has been reported in several cases. In Table 1 we give the mean absolute value of divergence in each of the five vertical modes, and at each model level, for the uninitialized analysis (in column 2) and after initialization of an increasing number of modes. The equivalent depths of the five vertical modes are 10398, 494, 94, 20 and 3·4 metres. All values in Table 1 are for the D-grid and two initialization iterations are applied in each case. The total divergence decreases consistently as more modes are initialized. It is noteworthy that the iteration procedure converges with all modes initialized; the scheme was run for 24 iterations and the fields after 4, 8, 16 and 24 iterations were virtually the same. This is in contrast to results reported for other methods (e.g. Williamson and Temperton 1981) where attempts to initialize the higher modes led to divergence.

The initialization using LASER includes a component (Eq. 25) which determines the change in surface pressure explicitly. This removes an indeterminacy found in many previously reported methods. For example, Temperton and Williamson (1981) assume a linear relationship between changes in $\log p_s$ and modified geopotential G, and Daley (1979) uses a variational formulation to remove the indeterminacy. When the slow

TABLE 1. MEAN ABSOLUTE DIVERGENCE IN EACH MODE AND AT EACH LEVEL OF LASER FOR THE UNINITIALIZED ANALYSIS (COLUMN 2) AND AFTER INITIALIZATION OF DIFFERENT NUMBERS OF VERTICAL MODES. UNITS ARE $10^{-6}s^{-1}$.

	Number of vertical modes initialized					
	0	1	2	3	4	5
Mode						
$m = 1$	9·23	0·95	0·90	0·90	0·90	0·90
$m = 2$	7·52	7·52	1·53	1·54	1·55	1·55
$m = 3$	9·87	9·87	9·87	2·65	2·68	2·70
$m = 4$	5·84	5·84	5·84	5·84	2·90	2·92
$m = 5$	2·97	2·97	2·97	2·97	2·97	1·79
Level						
$l = 1$	10·60	7·24	2·78	1·66	1·67	1.68
$l = 2$	10·00	6·05	6·01	2·75	2·11	2·15
$l = 3$	6·26	5·13	2·98	3·30	1·63	1·54
$l = 4$	6·81	6·68	3·80	2·55	2·62	1·62
$l = 5$	7·46	7·65	5·00	3·56	2·93	2·73

equations are used in forecasting, the explicit changes in surface pressure must be calculated from (25). It seems most natural to use the same procedure for initialization, which is what we have done.

4. CONCLUDING REMARKS

A multi-level model, LASER, based on the slow equations, has been formulated. The slow system comprises prognostic equations for potential vorticity and surface pressure and diagnostic relationships for the remaining variables. The goal in developing this model is to construct a system for hourly analysis and short-range forecasting. Since the slow equations are free of high-frequency solutions, it is hoped that they may be used to assimilate observational data at frequent intervals without repeated initialization and without data shock.

As a first step, the slow-equation model has been used to initialize data for a primitive-equation forecast. The diagnostic components of the slow system, the balance and imbalance equations, are similar to those used in the implicit normal-mode method. This method has recently been shown to yield results very similar to the explicit normal-mode method (McGregor and Bourke 1988). It has also been applied to a spectral barotropic model (Temperton 1989). In this paper we have shown that the technique provides a satisfactory method of initialization for a baroclinic limited-area model. The normal modes of such a model are generally unknown, as the horizontal variables are not separable. The method proposed here provides a practicable solution to the problem of initialization for such models.

We hope to report at a future time on the use of the model LASER in forecasting mode. Preliminary studies have indicated that the errors of forecasts with this model, while modest, may be too large to be tolerated in an operational context. The source of these errors does not appear to be the approximations made in deriving the slow system, but the treatment of the boundaries. A number of variations to the boundary formulation described in section 3 above have been tried, but, to date, no completely satisfactory formulation has been found. The boundary conditions used in this study are adequate for the initialization problem, but apparently not for forecasting. There is also some evidence of errors resulting from the present treatment of orography, and methods of improving this will be investigated.

Acknowledgement

The authors wish to thank Dr Andrew Staniforth for helpful comments on an earlier version of this paper.

Appendix

List of variables and constants

a	radius of the earth ($6{\cdot}371\times10^6$m)
c_p	isobaric specific heat ($1004{\cdot}6\,\mathrm{J\,kg^{-1}K^{-1}}$)
$\mathbf{E}$	vertical mode eigenvector matrix
f	Coriolis parameter ($2\Omega \sin\theta$)
G	modified geopotential ($\Phi+RT^0 \ln p_s$)
g	acceleration due to gravity ($9{\cdot}80665\,\mathrm{m\,s^{-2}}$)
$\mathbf{M}$	vertical coupling matrix (Eq. (14))
p	pressure (Pa)
p_s	surface pressure (Pa)
R	gas constant ($287{\cdot}04\,\mathrm{J\,kg^{-1}\,K^{-1}}$)
T	temperature (K)
T^0	mean temperature (K)
t	time (s)
u	zonal component of velocity ($\mathrm{m\,s^{-1}}$)
v	meridional component of velocity ($\mathrm{m\,s^{-1}}$)
δ	divergence ($\mathrm{s^{-1}}$)
ε	geostrophic imbalance ($\nabla^2 G - f\zeta$)
ζ	vorticity ($\mathrm{s^{-1}}$)
θ	latitude (radians)
λ	longitude (radians)
σ	vertical coordinate (p/p_s)
σ_T	value of σ at the top of the atmosphere
$\dot{\sigma}$	vertical velocity ($d\sigma/dt$)
Φ	geopotential ($\mathrm{m^2\,s^{-2}}$)
Φ_s	surface geopotential ($\mathrm{m^2\,s^{-2}}$)
χ	velocity potential ($\mathrm{m^2\,s^{-1}}$)
ψ	streamfunction ($\mathrm{m^2\,s^{-1}}$)
Ω	angular speed of the earth ($7{\cdot}292\times10^{-4}\mathrm{s^{-1}}$)

References

Bourke, W. and McGregor, J. L. 1983 A nonlinear vertical mode initialization scheme for a limited area prediction model. *Mon. Weather Rev.*, **111,** 2285–2297

Charney, J. G. 1962 Integration of the primitive and balance equations. Pp. 131–152 in *Proc. Intl. Symp. on NWP.* Published by Japanese Meteorological Agency, Ote-machi, Chiyoda-ku, Tokyo 100

Concus, P. and Golub, G. H. 1973 Use of fast direct methods for the efficient numerical solution of non-separable elliptic equations. *SIAM J. Numer. Anal.*, **10,** 1103–1120

Daley, R. 1979 The application of nonlinear normal mode initialization to an operational forecast model. *Atmos. Ocean*, **17,** 97–124

Juvanon du Vachat, R. 1986 A general formulation of normal modes for limited area models; application to initialization. *Mon. Weather Rev.*, **114,** 2478–2487

Lynch, Peter
1988 Deducing the wind from the vorticity and divergence. *Mon. Weather Rev.*, **116,** 86–93
1989 The slow equations. *Q. J. R. Meterol. Soc.*, **115,** 201–219

Machenhauer, B.
1977 On the dynamics of gravity oscillations in a shallow water model, with applications to normal mode initialization. *Beitr. Phys. Atmos.*, **50,** 253–271

McDonald, A.
1986 A semi-Lagrangian and semi-implicit two time-level integration scheme. *Mon. Weather Rev.*, **114,** 824–830

McDonald, A. and Bates, J. R.
1987 Improving the estimate of the departure point in a two time level semi-Lagrangian and semi-implicit scheme. *ibid.*, **115,** 737–739

McGregor, J. L. and Bourke, W.
1988 A comparison of vertical mode and normal mode initialization. *ibid.*, **116,** 1320–1334

Sangster, W. E
1960 A method of representing the horizontal pressure force without reduction of pressures to sea level. *J. Meteorol.*, **17,** 166–176

Sweet, R. A.
1977 A cyclic reduction algorithm for solving block tridiagonal systems of arbitrary dimension. *SIAM J. Numer. Anal.*, **14,** 706–720

Temperton, C.
1988 Implicit normal mode initialization, *Mon. Weather Rev.*, **116,** 1013–1031
1989 Implicit normal mode initialization for spectral models. *ibid.*, **117,** 436–451

Temperton, C. and Williamson, D. L.
1981 Normal mode initialization for a multi-level grid point model. Part 1: Linear aspects. *ibid.*, **109,** 729–743

Williamson, D. L. and Temperton, C.
1981 Normal mode initialization for a multi-level gridpoint model. Part II: Nonlinear aspects. *ibid.*, **109,** 744–757